APPENIX I

Model-In Project Logo

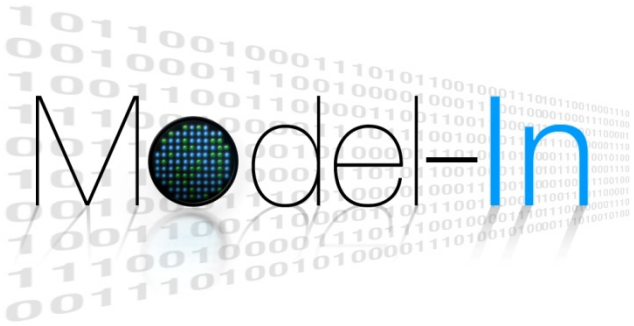

APPENDIX 2

List of Model-In Beneficiaries

	Beneficiary	Beneficiary Short name	Address	Contact name
1	University of Oxford	UOXF.H5	The Chancellor, Masters and Scholars of the University of Oxford University Offices Wellington Square Oxford OX1 2JD UK	Dr. Irina Udalova; Irina.udalova@kennedy.ox.ac.uk
2	Imperial College London	Imperial	Participation terminated as of 31/07/2011	
3	Université Joseph Fourier	UJF	621 Avenue Centrale, Domaine Universitaire 38041 Grenoble France	Dr. S. Dimitrov Stefan.dimitrov@ujf-grenoble.fr
4	Ecole Normale Supérieure de Lyon	ENSL	46 Allee d'Italie 69364 Lyon France	Dr. D. Angelov Dimitar.anguelov@ens-lyon.fr
5	Università Vita-Salute San Raffaele	USR	Via Olgettina 58 20132 Milano Itlay	Prof. M. Bianchi bianchi.marco@hsr.it
6	Istituto Europeo di Oncologia	IEO	Via Filodrammatici 10 20121 Milano Italy	Dr. G. Natoli gioacchino.natoli@ifom-ieocampus.it
7	Weizmann Institute	Weizmann	Herzel Street 76100 Rehovot Israel	Dr. E. Segal eran.segal@weizmann.ac.il
8	The Hebrew University of Jerusalem	HUJI	Givat Ram Campus 91904 Jerusalem Israel	Prof. N. Friedman nir@cs.huji.ac.il
9	Universität zu Köln	UzK	Albertus-Magnus-Platz 50923 Köln Germany	Prof. M. Pasparakis pasparakis@uni-koeln.de
10	Oxford Nanolabs	ONL	Begbroke Science Park, Sandy Lane, Kidlington Oxford OX5 1PF UK	Dr. S. Willcocks Spike.Willcocks@nanoporetech.com

11	IC Consultants	ICON	IC Consultants 58 Prince's Gate London SW7 2PQ	Dr. Kornelia Jumel k.jumel@imperial.ac.uk

APPENDIX 3

Figures and tables referred to in the Scientific Report

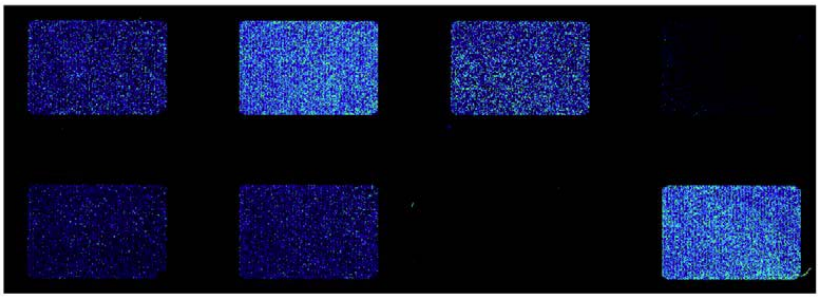

Figure: Scanning of an 8 x 15K array after hybridation with 8 different NF-kB proteins. Protein from left to right and then top to bottom: RelAp50, RelAp52, p52, RelA, RelBp50, RelBp52, p50 and cRelp50

RelBp50	0.84							
RelAp50	0.74	0.71						
RelA	0.77	0.52	0.75					
p50	0.68	0.69	0.94	0.65				
p52	0.75	0.66	0.82	0.71	0.68			
RelBp52	0.76	0.72	0.92	0.73	0.86	0.86		
RelAp52	0.77	0.70	0.89	0.73	0.80	0.90	0.95	
cRelp52	0.78	0.64	0.85	0.79	0.73	0.91	0.93	0.94
	cRelp50	**RelBp50**	**RelAp50**	**RelA**	**p50**	**p52**	**RelBp52**	**RelAp52**

Table 1: Pairwise comparison between pairs of NF-kB proteins using correlation coefficients

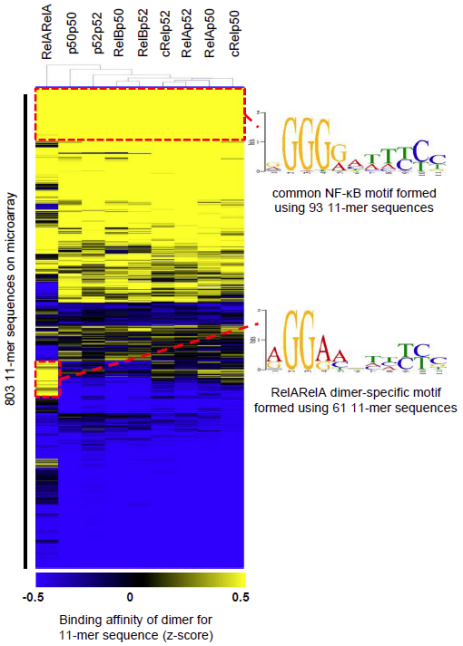

Figure: Heat-map illustration of binding profiles obtained from microarray-analysis of dimers. Within the heat-map, probes that contain the 803 11-mer sequences and represent "k-mer" space given by the consensus RGGRNNHHYYB can be found as rows whilst the nine NF-κB dimers have been organized into columns. A graded colour-scheme has been used to represent the ranked affinities of a dimer for a probe. From lightest to darkest this corresponds to decreasing affinity. Hierarchical clustering was used to describe relationships between binding profiles of the different dimers (Euclidean distance-correlation; complete linkage analysis). The profile of RelARelA was largely distinct from those of the other eight dimers.

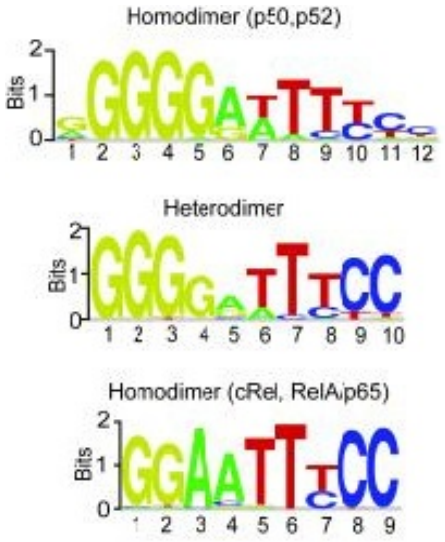

Figure: Three DNA-binding specificity clusters (i.e., class) were identified that correspond to three NF-κB dimer groups: p50,p52 homodimers, heterodimers and c-Rel,RelA homodimers. Representative DNA binding site motifs were determined for each dimer class using the top 25 highest-scoring κB sites bound by each group member

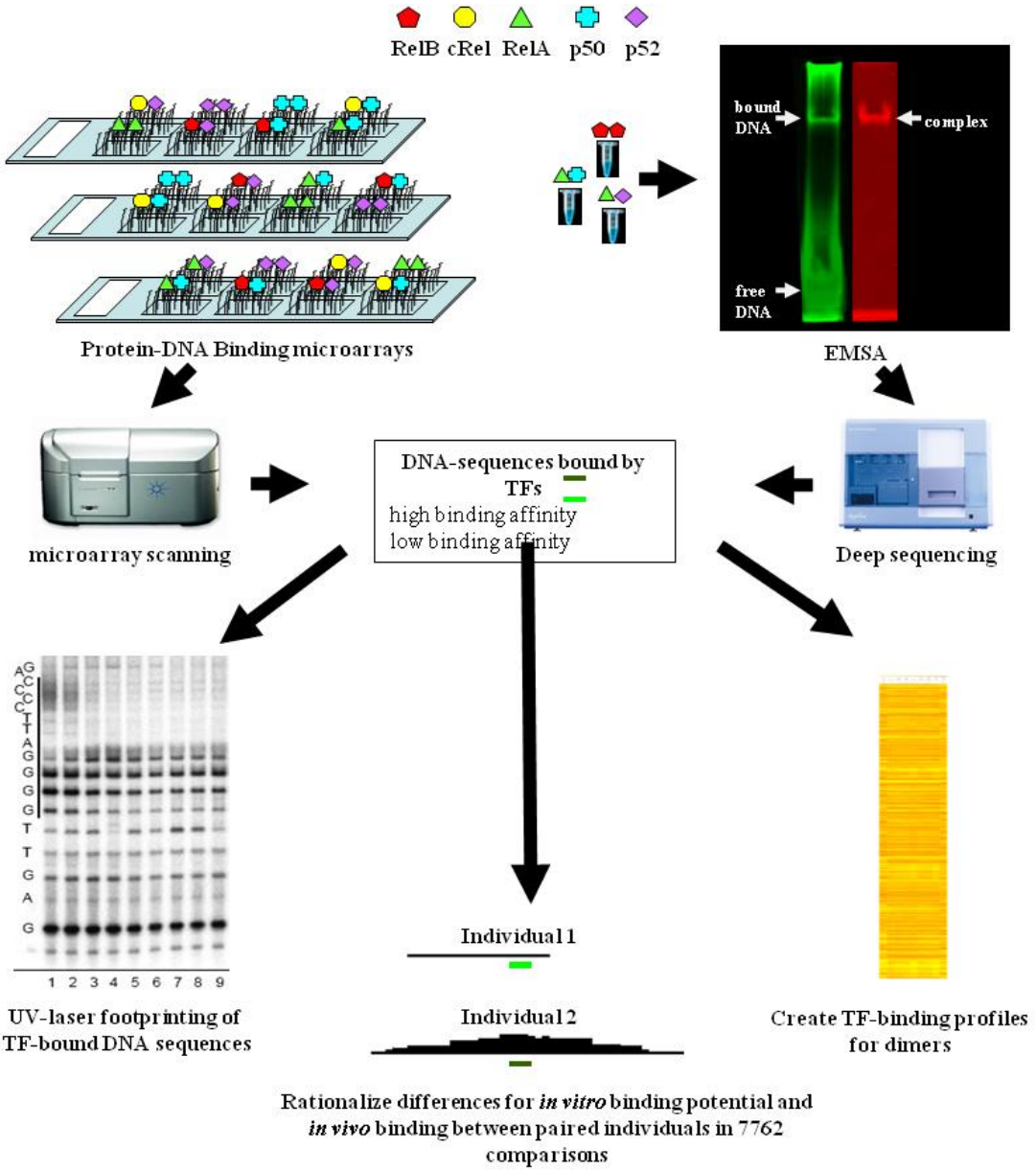

Figure: EMSA SEQ workflow

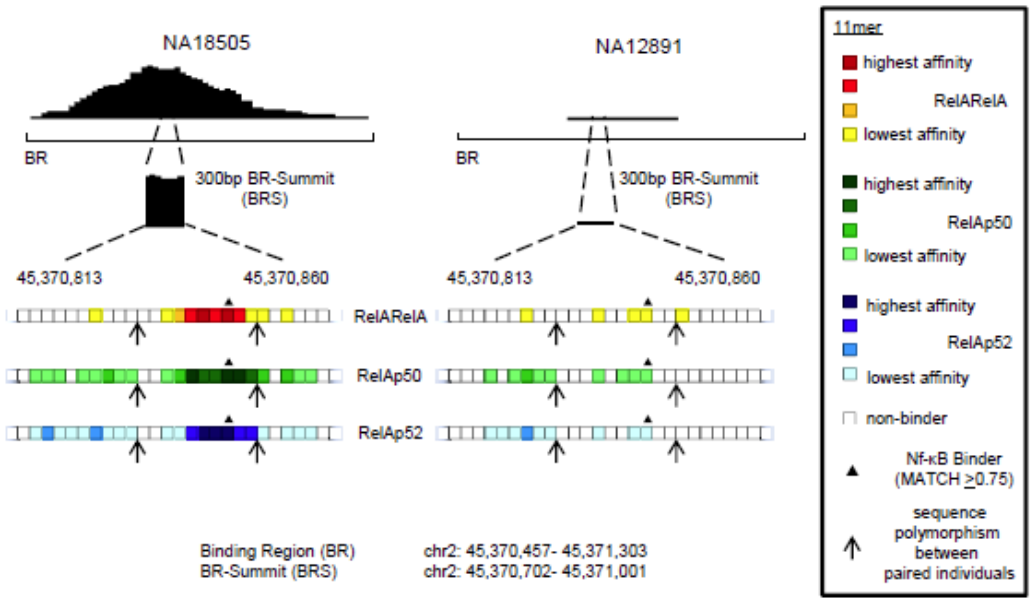

Figure: Mapping of EMSA-seq derived sequences within ChIP-seq peaks. For visualization purposes, the intensity of the colouration used during mapping is reflective of the binding affinity of a NF-kB dimer for 11-mer sequences identified by EMSA-Seq. The NF-κB binding potential of a BRS was then calculated by adding up the in vitro binding affinities of a set of dimer-specific 11-mers, either the homodimer or a heterodimer of RelA. Using data from the 1000 Genomes Project, we identified polymorphisms, if any, within the BRSs of paired individuals. Polymorphisms may or may not alter the composition of 11-mer sequences within the BRS of an individual. For example, as a direct consequence of two polymorphisms individual NA18505 has higher NF-κB binding potential compared to individual NA12891 and this corresponds to a greater extent of in vivo NF-κB binding observed.

Table 1

11-mer sequence	MATCH_score	RelARelA			RelAp50			RelAp52		
		Microarray Binding affinity (z-score)	EMSA-Seq Binding affinity (z-score)	UV-laser footprint Binding affinity (K_d)	Microarray Binding affinity (z-score)	EMSA-Seq Binding affinity (z-score)	UV-laser footprint Binding affinity (K_d)	Microarray Binding affinity (z-score)	EMSA-Seq Binding affinity (z-score)	UV-laser footprint Binding affinity (K_d)
AGGAAATTCCG	0.86	3.70	40.90	3.25	1.20	20.42	4.60	0.55	13.00	1.70
AGGGGGATCTG	0.49	non-binding	non-binding	non-binding	2.39	23.10	10.50	1.76	18.35	2.00
AGGGGAAGTTA	0.43	n.a.	3.78	non-binding	n.a.	35.41	26.00	n.a.	27.50	20.00
CTGGGGATTTA	0.29	n.a.	10.84	non-binding	n.a.	24.17	16.00	n.a.	19.54	13.80

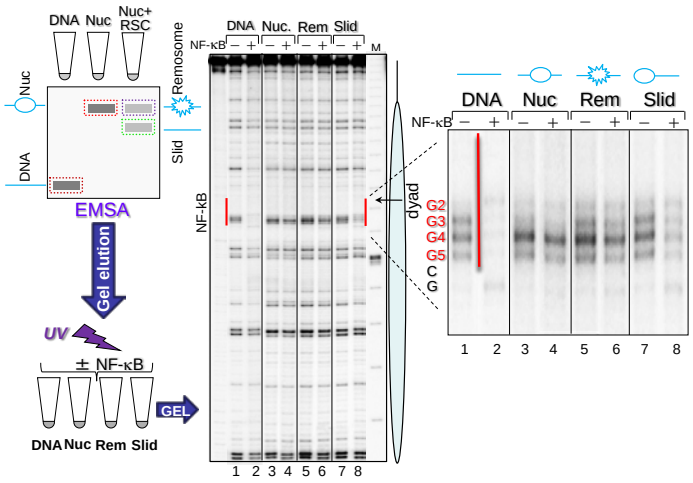

Figure: NF-kB is unable to bind to both unremodeled and remodeled nucleosomes.

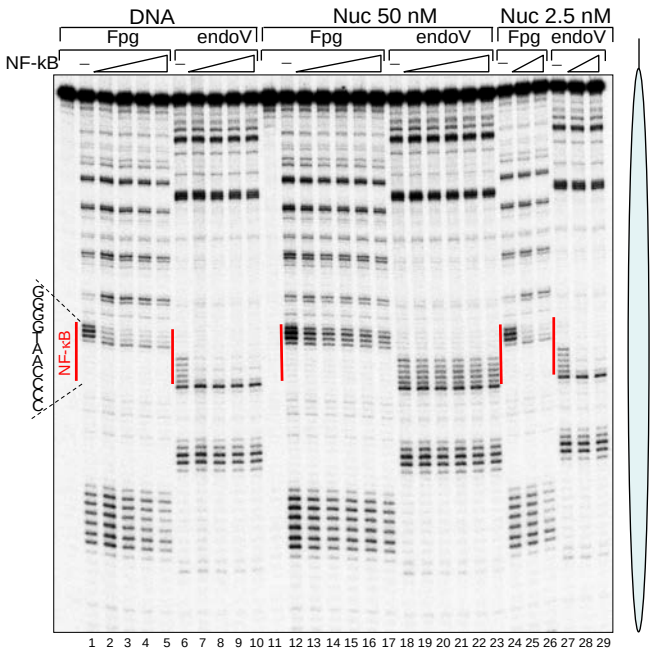

Figure: Nucleosome dilution driven H2A-H2B dimers eviction allows binding of NF-kB to the nucleosome core

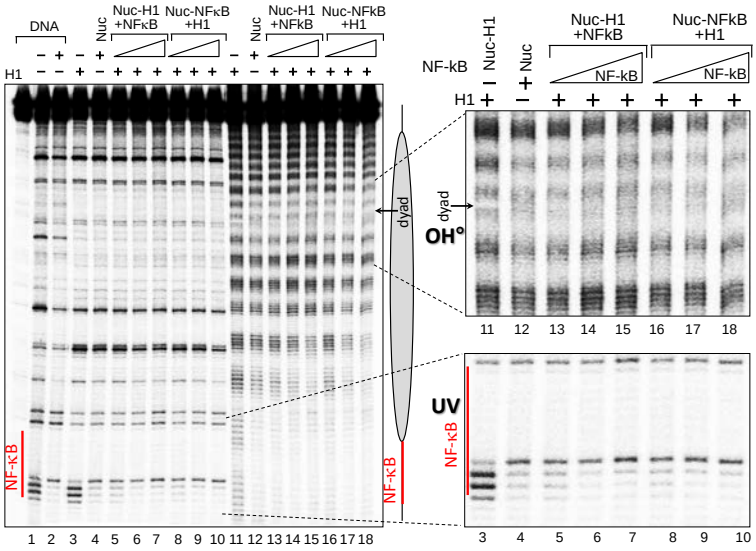

Figure: NF-kB displaces H1 from the chromatosome and prevents its binding.

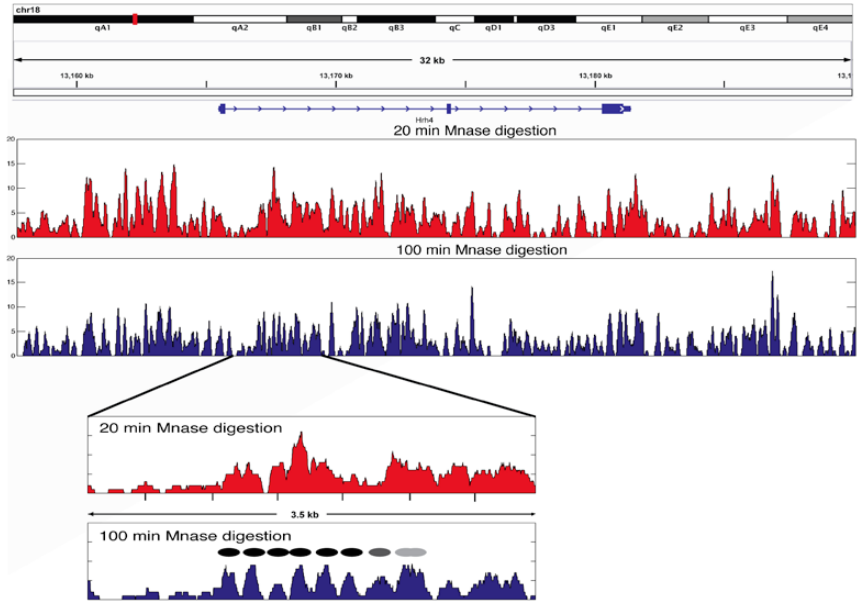

Figure: Coverage plot over a ~30kb genomic region. Inset: zoom in onto a 3.5kb region. The height of the graph denote level of coverage of each basepair by a nucleosome protected segment.

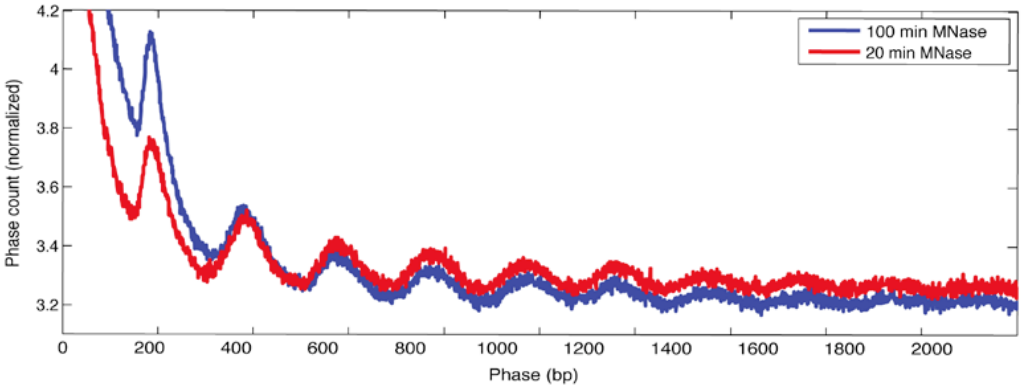

Figure: Phase correlation (y-axis) between coverage at different interval (x-axis). Ordered nucleosome positions would show higher counts at intervals that are multiples of nucleosome-nucleosome distance.

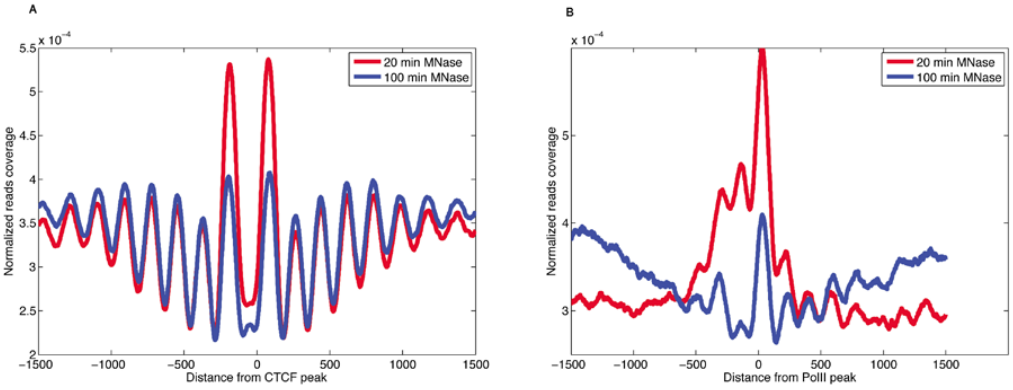

Figure: Average nucleosome coverage around CTCF binding sites (enhancers). **B:** Average nucleosome coverage around peaks of RNA Polymerase II (promoters).

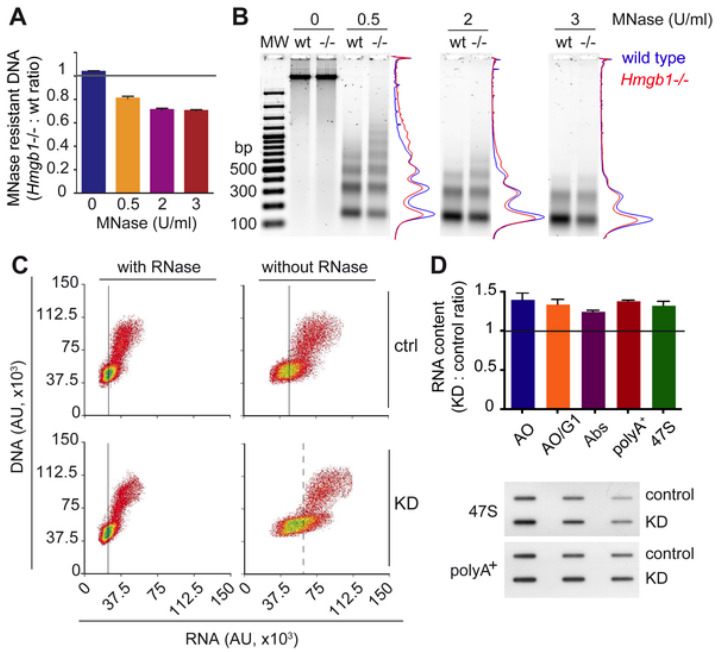

Figure: cells lacking HMGB1 have fewer nucleosomes and more transcripts. (A) Residual (nucleosome-protected) DNA obtained from *Hmgb1*−/− and wild type MEFs after digestion with increasing MNase concentrations. (B) Electrophoretic separation and densitometric analysis of DNA samples from 250,000 wild type and *Hmgb1*−/− MEFs after digestion with MNase. MW: 100 bp ladder. (C) FACS analysis of HeLa control (upper panels) and KD cells (lower panels) stained with Acridine Orange (AO), with or without prior RNase treatment (left and right, respectively). Fluorescence from AO bound to DNA (*y*-axis, 530/30 nm) and to RNA (*x*-axis, 610/20 nm). Black vertical lines (continuous and dashed) indicate the arithmetic means of RNA fluorescence in G1 cells. (D) Quantification of total RNA content in control and KD HeLa cells by FACS (cycling and G1) and by 260 nm absorbance of RNA extracted from a defined number of cells. Quantification of polyA$^+$mRNA and 47S rRNA precursor by RNA slot blot hybridization with specific probes.

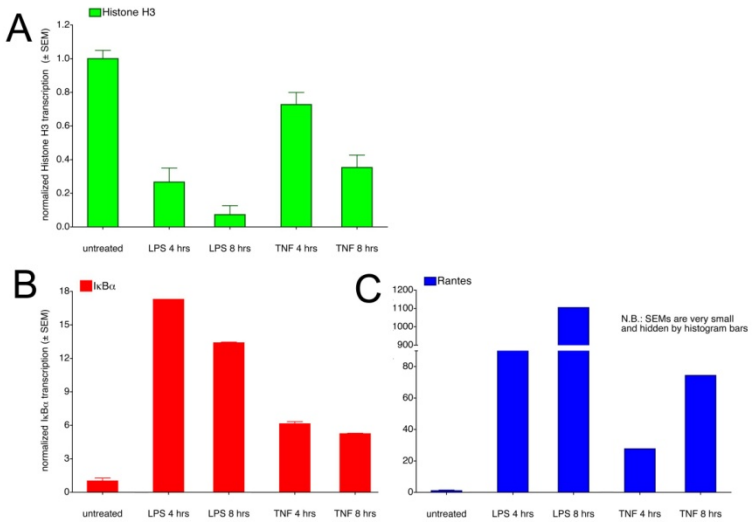

Figure: Transcription fold change of Histone H3 (green), I s in (red) and Rantes (blue) ge mouse macrophages stimulated with either LPS or TNF- for 4 or 8 hrs. Data are normalized setting the transcription level in unstimulated cells equal to 1. Representative experiment out of 5 performed.

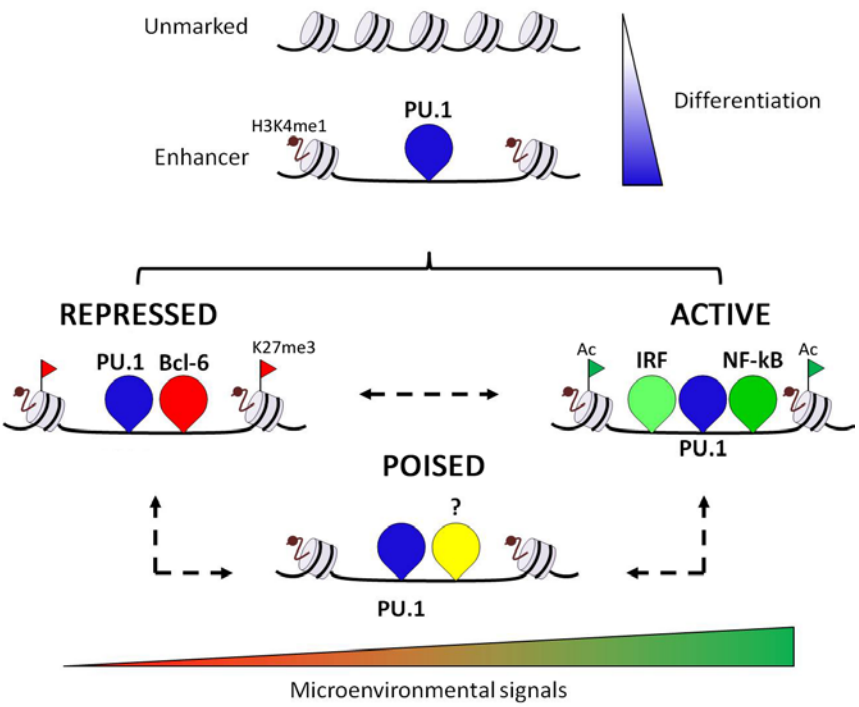

Figure: The macrophage-specific transcription factor PU.1 is constitutively bound to enhancers.

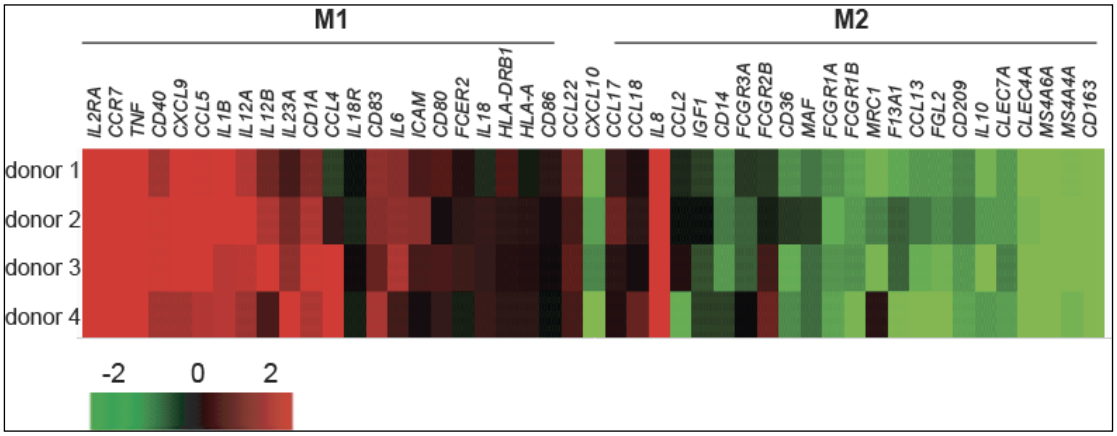

Figure: M2- macrophages from 4 different donors were infected with adenoviral vectors encoding IRF5 or empty vector (pENTR) and global mRNA expression was analysed using Illumina HumanHT-12 Expression BeadChips. Heatmaps showing the fold change in M2+IRF5 cells relative to M2 cells at 0hr for sets of M1 and M2-specific genes. Red indicates higher expression in M2+IRF5 and green indicates higher expression in M2 (scale shows the log2 fold change). M1-specific genes tend to be more highly expressed in M2+IRF5 cells whereas M2-specific genes are downregulated by IRF5.

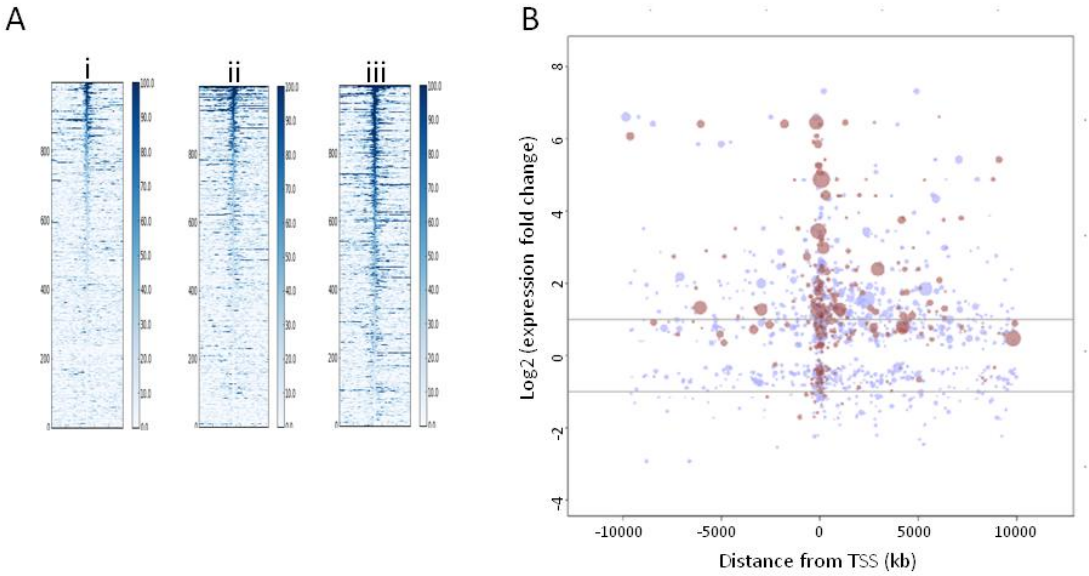

Figure: (A) The ChIP-seq datasets for *(i)* RelA , *(ii)* IRF5 and *(iii)* RelA_with_IRF5 were each aligned with respect to the centre of the PolII intervals and sorted by the length of the RelA marked regions. 1000 representative intervals are shown. (B) Bubble plot representation of RelA binding sites around differentially regulated genes. The plots indicate the position of ChIP-Seq intervals with respect to the closest transcription start site *(x-axis)* and the observed fold change *(y-axis)* in microarray expression experiments. The size of a bubble denotes the strength of the ChIP-Seq peak. *Red bubbles*: RelA_with_IRF5; *Blue Bubbles*: RelA_withoutIRF5

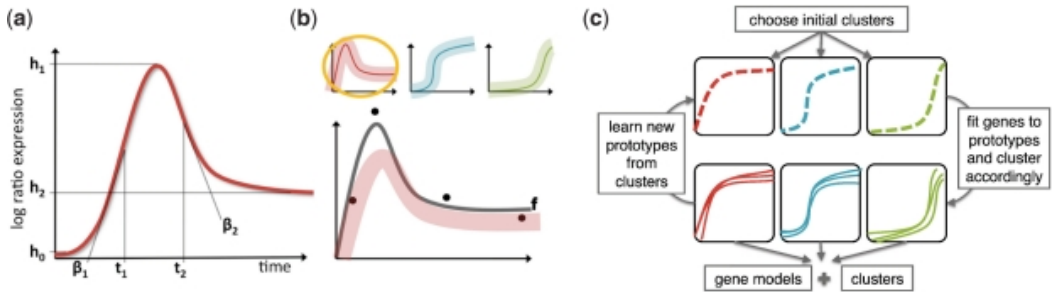

Figure.: An integrative clustering-modeling algorithm. (A) The *impulse model* capturing a two-phase temporal response by a product of two sigmoids, with parameters: onset time (*t*1), offset time (*t*2), the original baseline height (*h*0), peak response height (*h*1), new baseline height (*h*2), onset rate (β1) and offset rate (β2). (B) Fitting the model to the data with mixture priors on the parameters (bottom), which are distinct prototypes of responses (top). (C) A scheme describing our integrative clustering and modeling algorithm DynaMiteC: (i) Choosing initial clusters. (ii) Iterating between optimizing the fit to the genes and optimizing the prototypes. (iii) The resulting models per gene and clusters.

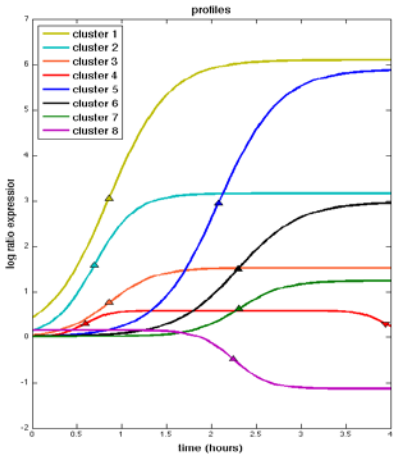

Figure: Dynamical modules of pathogen response. Eight dynamical response prototype found in the LPS response in mouse macrophages, by a combined analysis of time series data in wild-type and NF-kB knockout cells.

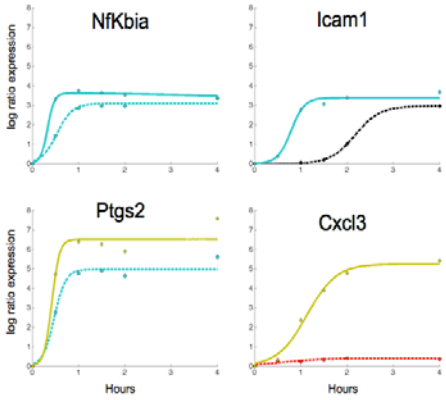

Figure: Effects of NF-kB on the dynamic expression pattern of genes. Four different examples for comparison of the dynamic expression pattern of genes. Showing the dynamic pattern in the wild-type (solid line) and in the NF-kB knockout (dashed line). The color of the line is according to the response prototype the gene is classified to (color scheme as in Figure above).

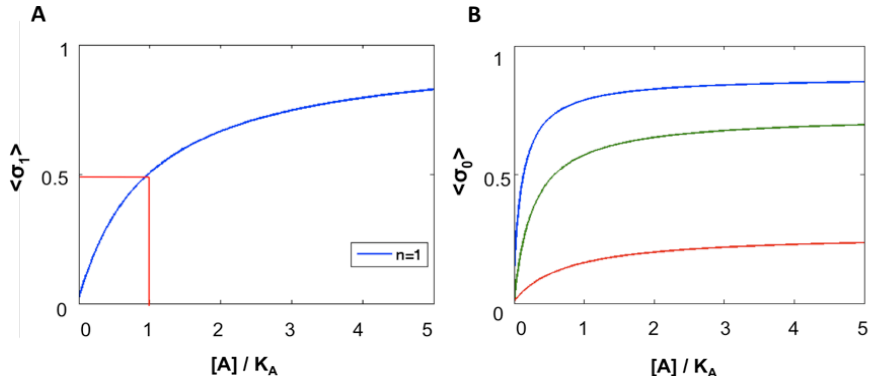

Figure: Model predictions in the case where only one NF-kB binding site is present (n=1). (A) Mean NF-kB binding site occupancy as a function of NF-kB nuclear concentration. (B) Mean Pol II occupancy on the core promoter as a function of NF-kB nuclear concentration. Blue: J=2k_BT, L=-4k_BT; Red: J=5k_BT, L=-4k_BT; Green: J=5k_BT, L=-6k_BT. Concentrations were renormalized to the NF-kB binding constant.

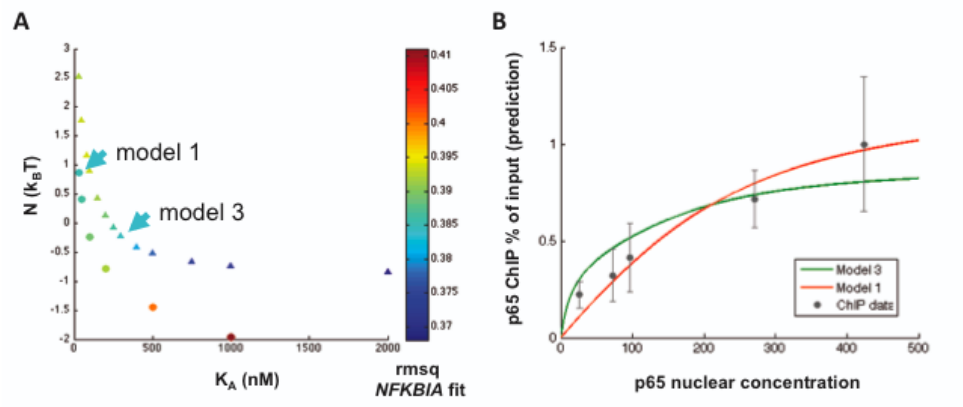

Figure: Equivalent model parameterizations return experimentally distinguishable predictions.(A) The root-mean-square values of the fits to the *NFKBIA* profile obtained with Model 1 (circles) and Model 3 (triangles) are plotted as a function of the imposed value of the NF-kB binding constant K_A and the best estimate of the free parameter N (controlling the strength of NF-kB binding cooperativity). The fit was performed with 6 kB sites in the *NFKBIA* promoter. Markers are colored according to the rmsq value (red: bad fit; blue: good fit). See Tables 1 and 3 in the supplementary Analysis and fitting of transcriptional induction profiles to compare the rmsq, N and K_A values. Arrowheads mark two parameter sets that return a fit with rmsq≈0.385. (B) The two parameter sets marked in panel A were used to predict the p65 occupancy profile on the cluster of 6 sites in the promoter. The two predictions show remarkably different rmsq values from the ChIP data, shown as gray markers (rmsq=0.0021 for Model1, 0.0012 for Model 3).

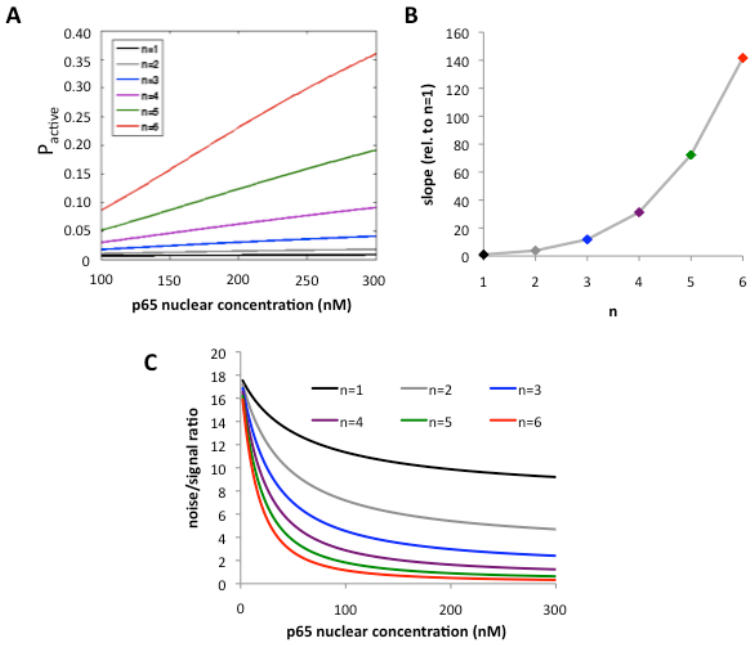

Figure: The number of NF-kB binding sites impacts on the dynamic range of transcription and the intrinsic transcriptional noise. (A) The number of kB sites determines the sensitivity of the transcriptional response to changes in NF-kB concentration. We calculated the transcriptional activation of genes with 1 to 6 kB promoter-proximal NF-kB binding sites under the experimentally determined conditions of additive Pol II recruitment in the absence of NF-kB binding cooperativity (K_A=200 nM), as a function of p65 nuclear concentration. The plot shows a magnification of the linear part of the curves, in the 100-300 nM range. The sensitivity to changes in TF concentration (i.e. the slope of the curve) increases when increasing the number of kB sites. (B) The slope of the curves shown in panel A was renormalized to the slope of the n=1 case, then potted against the number of kB sites. Increasing the number of sites from 1 to 6 leads to a dramatic increase in the sensitivity to changes in NF-kB concentration. (C) The intrinsic component of transcriptional noise, identified as the magnitude of equilibrium fluctuations in Pol II occupancy of the core promoter at a given p65 concentration (please refer to the description of the model in the Supplementary Information), is dependent on the number of NF-kB binding sites. We plotted the noise over signal ratio (i.e. the ratio of the mean square deviation of Pol II occupancy, $\delta\sigma_0$, over the average Pol II occupancy $<\sigma_0>$) versus the p65 nuclear concentration, for genes with 1 to 6 NF-kB binding sites. As in panel A, we ran the model in the identified regime of additive Pol II recruitment in the absence of NF-kB binding cooperativity.

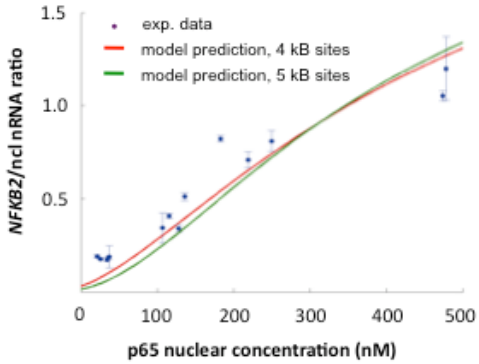

Figure: The experimental data and the predictions of Model 3 (in the identified regime of non-cooperative NF-kB binding and K_A=200 nM) concerning the transcriptional induction profile of *NFKB2*. The calculation was performed with 4 (red line) and 5 (green line) kB sites in the promoter.

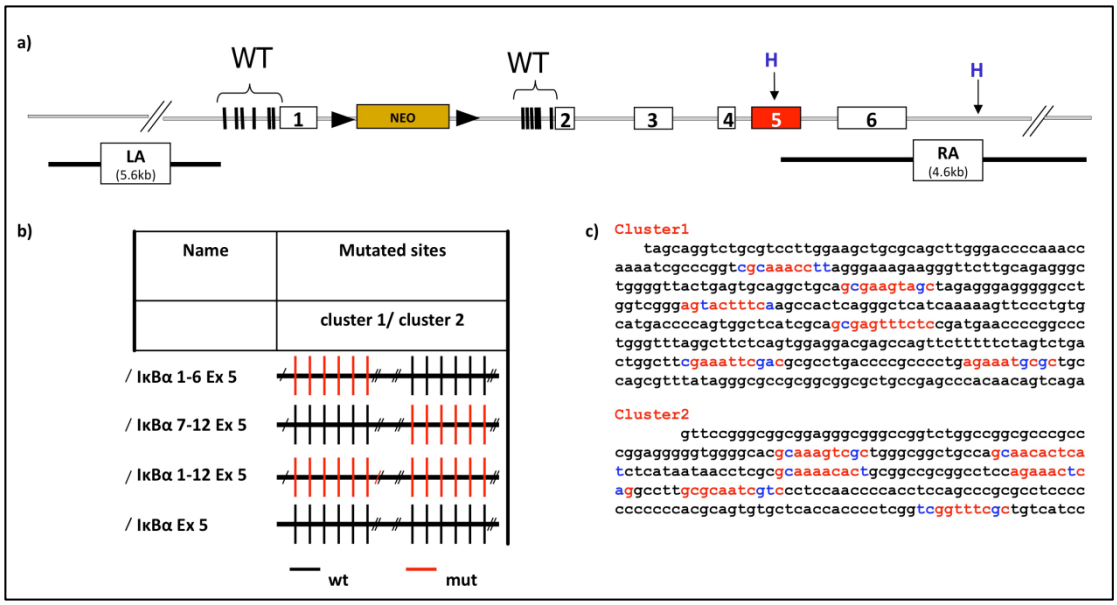

Figure: a) Basic targeting vector used for targeting the Nfkbia locus. LA and RA indicate the regions of homology used for homologous recombination b) Overview of the mutations generated, indicated with red colour are the mutated NF-κB binding sites in the two clusters. c) Mutations of NF-κB binding sites in the promoter "cluster1" and intronic "cluster2". Single NF-κB-sites are indicated in red. Exchanged nucleotides are indicated in blue.

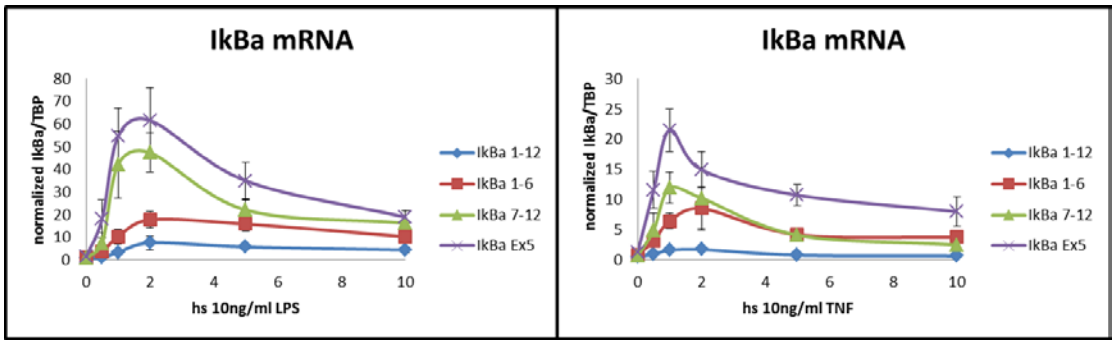

Figure: Analysis of the effect of NF-κB site mutations in LPS- or TNF induced transcription of IκBα. BMDMs homozygous for the indicated alleles were stimulated with 10 ng/ml LPS or 10 ng/ml TNF for the indicated time points. Transcription of IκBα was compared between the different genotypes using qPCR on isolated total RNA. Y-axis: Relative expression levels of IκBα mRNA after normalization with TBP as housekeeping gene; X-axis: hours after stimulation with LPS or TNF; Error bars indicate standard deviation of six biological replicates.

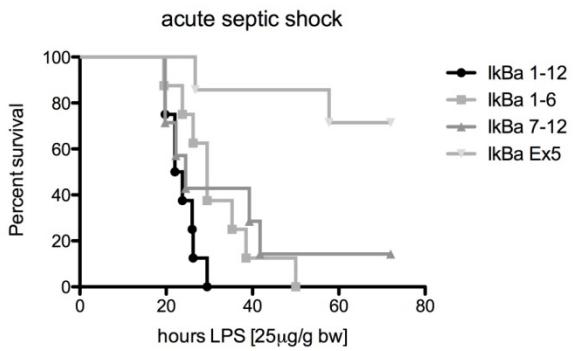

Figure: Seven female mice each from the IκBα 1-12 Ex5 and IκBα 1-6 Ex5 lines and six mice from the IκBα 7-12 Ex5 and IκBα Ex5 lines each were IP injected with 25µg/g bodyweight LPS and survival was monitored up to 72 hours post injection.

APPENDIX 4

Examples of dissemination activities

Figure 1: Announcement of the 2012 workshop in Athens, Greece

Modelling Inflammation (Model-In)

Model-In is a European Commission Seventh Framework Programme funded research collaboration, which aims to understand and quantitatively describe the transcriptional control of inflammatory responses. Over the past three years, the Europe-wide consortium which includes nine research partners from across the UK, France, Italy, Israel and Germany, and one UK based SME and is lead by Dr Irina Udalova at the Kennedy Institute for Rheumatology, has employed a unique combination of skills and state-of-the-art developed technologies to examine links between the sequence of individual transcription factor binding sites and tightly controlled expression of inflammatory genes, focusing on selected families of transcription factors (NF-κB, IRFs and AP-1 proteins).

BACKGROUND

Inflammation is a normal physiological response to infection or injury. However, an excessive or sustained inflammatory reaction can lead to extensive tissue damage and disability. The consequences of chronic inflammatory responses include a variety of diseases with huge social impact, ranging from autoimmune diseases, such as Crohn's and Multiple Sclerosis, to septic shock and cancer. A thorough understanding of the basic molecular mechanisms controlling inflammation is an essential requisite to the pharmacological tuning of harmful responses and the development of targeted anti-inflammatory drugs.

The inflammatory response is activated and maintained by the coordinated expression of hundreds of genes whose products (specific proteins called cytokines) recruit and activate white blood cells, increase vascular permeability and protect inflammatory and tissue cells from programmed cell death.

APPROACH

The process of gene expression begins with transcription, whereby information stored in a gene's DNA is transferred to a complementary messenger molecule called RNA. This fundamental step equips the cell with the ability to produce any protein expressed by the gene. Transcription, and thus gene expression, of many inflammatory cytokines is tightly controlled by transcription factors (TFs). Combinations of these trans-regulatory elements interact with regulatory DNA sequences along specific binding sites (TFBSs) to control which genes within the sequence are activated.

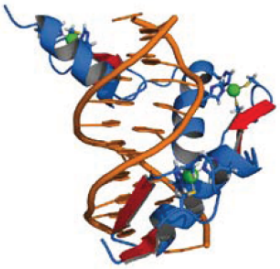

Transcription factors bind to DNA

Although this dynamic relationship is central to all inflammatory responses, relatively little is known about the location, properties and physiological behaviour of TFs and regulatory DNA elements, or how their interactions lead to normal or pathological outcomes. It is a key challenge of genomic biology to identify and characterise these regulatory elements and to model their function, in order to fully understand how a specific genomic organisation translates into regulated responses.

To address this challenge, the Model-In consortium has utilised a rational combination of quantitative *in vitro* and *in vivo* analyses, mathematical modelling and *in vivo* perturbation experiments, successfully generating new types of experimental data and building computational and functional genomic models of the inflammatory response.

Model-In

For further information contact the coordinator:
Dr. Irina Udalova
Kennedy Institute of Rheumatology
e-mail: irina.udalova@kennedy.ox.ac.uk
website: www.model-in.org

Figure 2: Article released in *The Parliament Magazine* which is aimed at UK and EU parliamentarians